

2021-2

A dual-functionality metalens to shape a circularly polarized optical vortex or a second-order cylindrical vector beam

Victor V. Kotlyar

Image Processing Systems Institute of the RAS – Branch of FSRC "Crystallography & Photonics" of the RAS, 151 Molodogvardeyskaya st., Samara 443001, Russia; Samara National Research University, 34 Moskovskoe shosse, Samara 443086, Russia

Sergey S. Stafeey

Image Processing Systems Institute of the RAS – Branch of FSRC "Crystallography & Photonics" of the RAS, 151 Molodogvardeyskaya st., Samara 443001, Russia; Samara National Research University, 34 Moskovskoe shosse, Samara 443086, Russia

Anton G. Nalimov

Image Processing Systems Institute of the RAS – Branch of FSRC "Crystallography & Photonics" of the RAS, 151 Molodogvardeyskaya st., Samara 443001, Russia; Samara National Research University, 34 Moskovskoe shosse, Samara 443086, Russia

Liam O'Faolain

Centre for Advanced Photonics and Process Analysis, Munster Technological University, Cork, Ireland; Tyndall National Institute, Cork, Ireland, liam.ofaolain@tyndall.ie

Maria V. Kotlyar

For this and additional works at: <https://sword.cit.ie/cappaart>
Centre for Advanced Photonics and Process Analysis, Munster Technological University, Cork, Ireland; Tyndall National Institute, Cork, Ireland, maria.kotlyar@mtu.ie

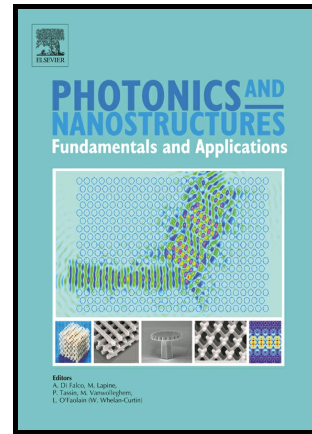
Recommended Citation

Kotlyar, V.V., Stafeev, S.S., Nalimov, A.G., O'Faolain, L. and Kotlyar, M.V. (2021). A dual-functionality metalens to shape a circularly polarized optical vortex or a second-order cylindrical vector beam. *Photonics and Nanostructures - Fundamentals and Applications*, [online] 43, p.100898. doi:<https://doi.org/10.1016/j.photonics.2021.100898>.

This Article is brought to you for free and open access by the Cappa Centre at SWORD - South West Open Research Deposit. It has been accepted for inclusion in Cappa Publications by an authorized administrator of SWORD - South West Open Research Deposit. For more information, please contact sword@cit.ie.

A dual-functionality metalens to shape a circularly polarized optical vortex or a second-order cylindrical vector beam

Victor V. Kotlyar, Sergey S. Stafeev, Anton G. Nalimov, Liam O’Faolain, Maria V. Kotlyar



PII: S1569-4410(21)00005-5

DOI: <https://doi.org/10.1016/j.photonics.2021.100898>

Reference: PNFA100898

To appear in: *Photonics and Nanostructures - Fundamentals and Applications*

Received date: 8 October 2020

Revised date: 22 December 2020

Accepted date: 28 January 2021

Please cite this article as: Victor V. Kotlyar, Sergey S. Stafeev, Anton G. Nalimov, Liam O’Faolain and Maria V. Kotlyar, A dual-functionality metalens to shape a circularly polarized optical vortex or a second-order cylindrical vector beam, *Photonics and Nanostructures - Fundamentals and Applications*, (2020) doi:<https://doi.org/10.1016/j.photonics.2021.100898>

This is a PDF file of an article that has undergone enhancements after acceptance, such as the addition of a cover page and metadata, and formatting for readability, but it is not yet the definitive version of record. This version will undergo additional copyediting, typesetting and review before it is published in its final form, but we are providing this version to give early visibility of the article. Please note that, during the production process, errors may be discovered which could affect the content, and all legal disclaimers that apply to the journal pertain.

A dual-functionality metalens to shape a circularly polarized optical vortex or a second-order cylindrical vector beam

Victor V. Kotlyar,^{1,2} Sergey S. Stafeev,^{1,2,*} Anton G. Nalimov^{1,2}, Liam O’Faolain^{3,4}, Maria V. Kotlyar^{3,4}

¹Image Processing Systems Institute of the RAS — Branch of FSRC "Crystallography & Photonics" of the RAS, 151 Molodogvardeyskaya st., Samara, 443001, Russia

²Samara National Research University, 34 Moskovskoe shosse, Samara, 443086, Russia

³Centre for Advanced Photonics and Process Analysis, Cork Institute of Technology, Cork, T12 P928, Ireland

⁴Tyndall National Institute, Cork, T12R5CP, Ireland

*sergey.stafeev@gmail.com

Abstract— Using e-beam lithography and reactive ion beam etching of a 120-nm amorphous silicon film, we fabricate a 30- μm spiral metalens that has a very short focal length that is equal to the incident 633-nm wavelength (numerical aperture about 1) and is composed of 16-sector subwavelength binary gratings with a 220-nm period. Its unique feature is that the metalens generates a left-hand circularly polarized optical vortex with topological charge 2 when illuminated by a left-hand circularly polarized light but generates a cylindrical second-order vector beam when illuminated by linearly polarized light. Both for linearly and circularly polarized light, an inverse energy flow occurs near the strong focus of the metalens. Transverse near-focus intensity distributions measured with a scanning near-field optical microscope are found to be in qualitative agreement with those obtained via the FDTD-aided numerical simulation. Thus, the near-focus reverse energy flow is experimentally confirmed to occur.

Keywords—metalens, metasurface, subwavelength grating, tight focusing, Poynting vector, Richards-Wolf formula

1. Introduction

The trend towards the miniaturization of optical elements has generated interest in optical metasurfaces, which are ultrathin-film optical elements that enable the amplitude, phase, and polarization of light to be controlled simultaneously. The most widely used optical elements – lenses based on metasurfaces, were proposed in Refs. [1–9], in which the desired characteristics were attained by using metalenses containing optical antennae. For example, antennae in the form of elliptical cylinders [2] and L-shaped antennae [4] have been proposed. Another way to control characteristics of a light field is through the use of subwavelength diffraction gratings: with the subwavelength grating being anisotropic, TE- and TM-waves will have different phases and amplitudes after passing through it. Based on this effect, analogs of conventional polarization converters and wave plates can be designed [10]. In particular, in a number of earlier papers, we experimentally characterized optical metasurfaces intended to generate a subwavelength focal spot. For instance, in Ref. [11], using a 16-sector metalens, linearly polarized incident light was converted into an azimuthally polarized optical vortex and focused into a subwavelength focal spot whose size was less than the diffraction limit. Obtaining focal spots of size below the diffraction limit is not the only remarkable effect that can be observed. Other recently discovered effects include multi-segmented light tunnels [12, 13], optical chains [14,15], and flat-top foci [16,17]. Previously, we have theoretically shown that by focusing light with a carefully selected

polarization state and phase it is possible to generate tight-focus regions where the Poynting vector is directed oppositely to the incident light [18–20].

The latest advances in the development of high-efficiency, high-NA metalenses have been set forth in Refs. [21-27], which deal with multifocus metalenses. Such metalenses are capable of generating an array of foci along the optical axis or in a transverse plane. In this work, rather than studying the multifocal properties of the metalens, we aim at demonstrating multi-functionality. Depending on the type of the illuminating beam, the metalens under study is able to generate in the focus a beam with either phase or polarization singularity.

In an earlier work [28], we reported on the design of a similar metalens, theoretically showing it to form a reverse energy flow at the focus and presenting a prototype metalens, which proved to be of inferior quality, preventing us from its detailed experimental characterization. Here, we report on the fabrication of a high-quality metalens, enabling an optical experiment to be conducted and results that prove the generation of the reverse energy flow in the tight focus to be obtained. The high quality of the metalens under analysis is corroborated by the good agreement between the results of the experiment and the rigorous numerical simulation. The use of a metalens with high NA enables the magnitude of the reverse energy flow to be increased.

Below, we discuss the fabrication and characterization of a metalens intended to generate a reverse energy flow in the focus. The metalens under study combines a spiral Fresnel zone plate with 633-nm focus and a 16-sectored polarization converter based on subwavelength binary diffraction gratings of period 220 nm and depth 120 nm. The multi-sectored polarizer converts an incident linearly polarized Gaussian beam into a cylindrical second-order vector beam, being also able to convert a right-hand circularly polarized Gaussian incident beam into a right-hand circularly polarized optical vortex with topological charge $m = -2$ and a left-hand circularly polarized Gaussian beam into a left-hand circularly polarized optical vortex with $m = +2$. Unlike our previous works dealing with metalenses based on subwavelength diffraction gratings [11, 28], this work reports on the fabrication and experimental characterization of a metalens specifically designed to create a reverse energy flow in the strong focus. A distinctive feature of the fabricated metalens is that after passing it, an arbitrary input beam with uniform polarization generates an on-axis near-focus reverse energy flow. It would be possible to generate similar intensity distributions with a combination of a 2nd-order liquid crystal q-plate [29] and a focusing microlens (100x, NA=0.95), as reported in Ref. [30]. Meanwhile, in this work, we propose using a single metalens capable of successfully replacing the 'q-plate plus microlens' combination. Therefore, the major finding of this work is that, through transverse intensity measurements, we have proven that the metalens generates either a circularly polarized optical vortex or a vortex-free cylindrically polarized optical beam. Besides, we have shown that in both cases, a reverse energy flow occurs in the focus.

2. Theoretical background

The operation of a spiral optical metasurface [28] can be schematically defined by the Jones matrix $R(\varphi) = \begin{pmatrix} \cos 2\varphi & -\sin 2\varphi \\ \sin 2\varphi & \cos 2\varphi \end{pmatrix}$, which describes the polarization vector rotation by a polar angle φ . When illuminated by a TE-wave (projection E_x of the incident E-field), the metasurface $R(\varphi)$ with $m=2$ produces the output second-order radial polarization:

$$\begin{pmatrix} \cos 2\varphi & -\sin 2\varphi \\ \sin 2\varphi & \cos 2\varphi \end{pmatrix} \begin{pmatrix} 1 \\ 0 \end{pmatrix} = \begin{pmatrix} \cos 2\varphi \\ \sin 2\varphi \end{pmatrix} \quad (1)$$

When illuminated by a TM-wave (projection E_y of the incident E-field), at the output is an azimuthally polarized second-order optical beam:

$$\begin{pmatrix} \cos 2\varphi & -\sin 2\varphi \\ \sin 2\varphi & \cos 2\varphi \end{pmatrix} \begin{pmatrix} 0 \\ 1 \end{pmatrix} = \begin{pmatrix} -\sin 2\varphi \\ \cos 2\varphi \end{pmatrix} \quad (2)$$

When illuminated by a right-handed circularly polarized beam (the incident field E_x+iE_y), the metasurface $R(\varphi)$ produces a right-handed circularly polarized optical vortex with topological charge $m=-2$:

$$\begin{pmatrix} \cos 2\varphi & -\sin 2\varphi \\ \sin 2\varphi & \cos 2\varphi \end{pmatrix} \begin{pmatrix} 1 \\ i \end{pmatrix} = \exp(-i2\varphi) \begin{pmatrix} 1 \\ i \end{pmatrix} \quad (3)$$

Finally, when illuminated by a left-handed circularly polarized beam (initial field E_x-iE_y), the metasurface $R(\varphi)$ produces a left-handed circularly polarized optical vortex with topological charge $m=2$:

$$\begin{pmatrix} \cos 2\varphi & -\sin 2\varphi \\ \sin 2\varphi & \cos 2\varphi \end{pmatrix} \begin{pmatrix} 1 \\ -i \end{pmatrix} = \exp(2i\varphi) \begin{pmatrix} 1 \\ -i \end{pmatrix} \quad (4)$$

A combination of the metasurface $R(\varphi)$ and a binary zone plate gives a metalens that focuses the fields in (1)-(4) at a given distance f . Expressions (1)-(4) suggest that the metalens converts an incident linearly polarized plane wave into a cylindrical second-order vector beam, a right-handed circularly polarized plane wave – into a right-handed circularly polarized optical vortex with topological charge $m = -2$, and, finally, a left-handed circularly polarized plane wave – into a left-handed circularly polarized optical vortex with $m = +2$.

Immediately behind the metalens, the circularly polarized optical vortex with $m=2$ is given by

$$\mathbf{E} = \frac{A(\theta)e^{i2\varphi}}{\sqrt{2}} \begin{pmatrix} 1 \\ i\sigma \end{pmatrix}, \quad \mathbf{H} = \frac{A(\theta)e^{i2\varphi}}{\sqrt{2}} \begin{pmatrix} -i\sigma \\ 1 \end{pmatrix}, \quad (5)$$

where $\sigma=1$ for right-handed circular polarization and $\sigma=-1$ for left-handed circular polarization. When such a vortex is tightly focused, the E- and H-vector components in the focus neighborhood can be derived using the Richards-Wolf formalism [31] :

$$\begin{aligned} E_x &= \frac{i}{2\sqrt{2}} \left(e^{i2\varphi} I_{0,2} + \gamma_+ e^{i4\varphi} I_{2,4} + \gamma_- I_{2,0} \right), \\ E_y &= \frac{-1}{2\sqrt{2}} \left(\sigma e^{i2\varphi} I_{0,2} - \gamma_+ e^{i4\varphi} I_{2,4} + \gamma_- I_{2,0} \right), \quad (6) \\ E_z &= \frac{1}{\sqrt{2}} \left(\gamma_+ e^{i3\varphi} I_{1,3} - \gamma_- e^{i\varphi} I_{1,1} \right), \end{aligned}$$

$$H_x = \frac{1}{2\sqrt{2}} \left(\sigma e^{i2\varphi} I_{0,2} + \gamma_+ e^{i4\varphi} I_{2,4} - \gamma_- I_{2,0} \right),$$

$$H_y = \frac{i}{2\sqrt{2}} \left(\sigma e^{i2\varphi} I_{0,2} - \gamma_+ e^{i4\varphi} I_{2,4} - \gamma_- I_{2,0} \right),$$

$$H_z = \frac{-i}{\sqrt{2}} \left(\gamma_+ e^{i3\varphi} I_{1,3} + \gamma_- e^{i\varphi} I_{1,1} \right),$$

where $\gamma_{\pm} = (1 \pm \sigma)/2$ ($\gamma_+ = \gamma_- = 1/\sqrt{2}$ at $\sigma = 0$),

$$I_{\nu,\mu} = \left(\frac{\pi f}{\lambda} \right)^{\nu} \int_0^{\theta_0} \sin^{\nu+1} \left(\frac{\theta}{2} \right) \cos^{3-\nu} \left(\frac{\theta}{2} \right) \cos^{1/2}(\theta) A(\theta) e^{ikz \cos \theta} J_{\mu}(x) d\theta, (7)$$

where λ is the incident wavelength, f is the focal length of an aplanatic system, $x = kr \sin \theta$, $J_{\mu}(x)$ is a Bessel function of the first kind, an $NA = \sin \theta_0$ is the numerical aperture. The (real) incident amplitude function $A(\theta)$ may be given by a constant (a plane wave) or a Gaussian beam.

Based on Eq. (6), expressions can be derived for the intensity distribution of a left-handed ($\gamma_+ = 0, \gamma_- = 1$) circularly polarized optical vortex in the focal plane:

$$I = I_x + I_y + I_z = |E_x|^2 + |E_y|^2 + |E_z|^2 = \frac{1}{4} (I_{0,2}^2 + I_{2,0}^2 + 2I_{1,1}^2). (8)$$

Similarly, an expression can be obtained for the longitudinal component of the Poynting vector $\mathbf{S} = \text{Re}[\mathbf{E}^* \times \mathbf{H}]$ in the focal plane when focusing a left-handed circularly polarized optical vortex with topological charge $m = 2$:

$$S_z = \frac{1}{4} (2I_{0,2}^2 - I_{2,0}^2). (9)$$

The Poynting vector (energy flow) is given by [31] $\mathbf{S} = [c/(8\pi)] \text{Re}[\mathbf{E} \times \mathbf{H}^*]$, where c is the speed of light in vacuum, $\mathbf{E} \times \mathbf{H}$ is the cross product, and $*$ stands for complex conjugation. Below, we omit the constant $c/(8\pi)$. From (8) and (9), it is seen that in the focal plane ($z=0$), the on-axis ($r=0$) intensity is positive and the energy flow is negative:

$$I(z=r=0) = \frac{1}{4} I_{0,2}^2, S_z = -\frac{1}{4} I_{0,2}^2. (10)$$

Below, we demonstrate that a reverse energy flow does occur in the focus of a metalens illuminated by the linearly (Eqs. (1), (2)) or circularly (Eqs. (3), (4)) polarized laser light.

3. Design, fabrication, and relief measurements of a metalens

Figure 1a depicts the metalens of interest. A detailed description of the design of such a metalens can be found in Ref. [28]. The metalens combines a sectorized wave-plate and a spiral Fresnel zone plate of focal length $f = \lambda = 633$ nm (numerical aperture: $NA \approx 1$). The wave-plate serves as a polarization converter of incident light, which is described by a Jones matrix $R(\varphi) = \begin{pmatrix} \cos 2\varphi & -\sin 2\varphi \\ \sin 2\varphi & \cos 2\varphi \end{pmatrix}$, where φ is the polar angle in the metalens plane.

The metalens under study was synthesized in amorphous silicon. As a rule, this material is utilized for lenses working in the infrared range [1, 2, 5, 7, 8], whereas for the visible frequencies titanium dioxide

TiO₂ [32–34], silicon nitride SiN [35] or gallium nitride GaN [36,37] are normally used. The highest efficiency (93%) was attained for the metasurface synthesized in a SiN_x film [38], but the metalens featured low NA. A metalens synthesized in an amorphous silicon film of thickness 250 nm with near-unit NA (NA=0.99) and focal length of $f=42\ \mu\text{m}$ was discussed in Ref. [39], but the metalens had low efficiency (10%). A number of papers reported on the use of silicon for the visible spectrum [6, 40]. Although silicon shows high absorption in the visible spectrum, the efficiency of optical metasurfaces, is shown to be higher than that of metals [4,9], reaching 12% in the case under analysis. The metalens proposed herein has a high-numerical aperture (NA=0.99) and short-focus length ($f = \lambda$), which requires a subwavelength period of the microrelief (of about 200 nm). Seeking to ensure a π -phase shift in the metalens relief and a possibly small etch-depth to period ratio (thus making the microrelief walls maximally vertical), we chose a film with the highest refractive index (amorphous silicon). The consequence of the choice of silicon was low efficiency in the visible spectrum. The metalens was not tested for the damage threshold, as we worked with low-power energies below 100mW. To attain high damage thresholds, a related metalens may be fabricated in a metal film, similar to Ref. [41].

In this work, to synthesize the metalens, a 120-nm thick amorphous silicon film (a-Si, refractive index, $n = 4.35 + i0.486$) was applied onto a transparent pyrex substrate ($n = 1.5$), which was then coated with a 150-nm ZEP resist layer. The resist was baked at 180 C°. To dissipate charge, a 10-nm aluminium coating was applied onto the sample surface. The binary pattern was transferred onto the resist by an 30KV electron beam. The sample was then developed in ZED-N50.

The template (Fig. 1a) was transferred from the resist onto the amorphous silicon by inductively coupled plasma (ICP) etching in a gaseous atmosphere of C₄F₈ and SF₆. A metalens image obtained with an electron microscope is depicted in Fig. 1(b). A magnified metalens fragment is shown in Fig. 1(c). The metalens diameter is 30 μm , the period of binary subwavelength gratings is 220 nm (110-nm valleys and 110-nm steps). The metalens microrelief depth of 120 nm equals the thickness of the amorphous silicon film. Spatially varying subwavelength diffraction gratings occupy 16 sectors, enabling the metalens to rotate the polarization of incident light by 16 different angles. A phase shift by π between the adjacent zones of a Fresnel spiral plate in the metalens (Fig. 1) is implemented with the adjacent local diffraction gratings that form oppositely directed polarization vectors.

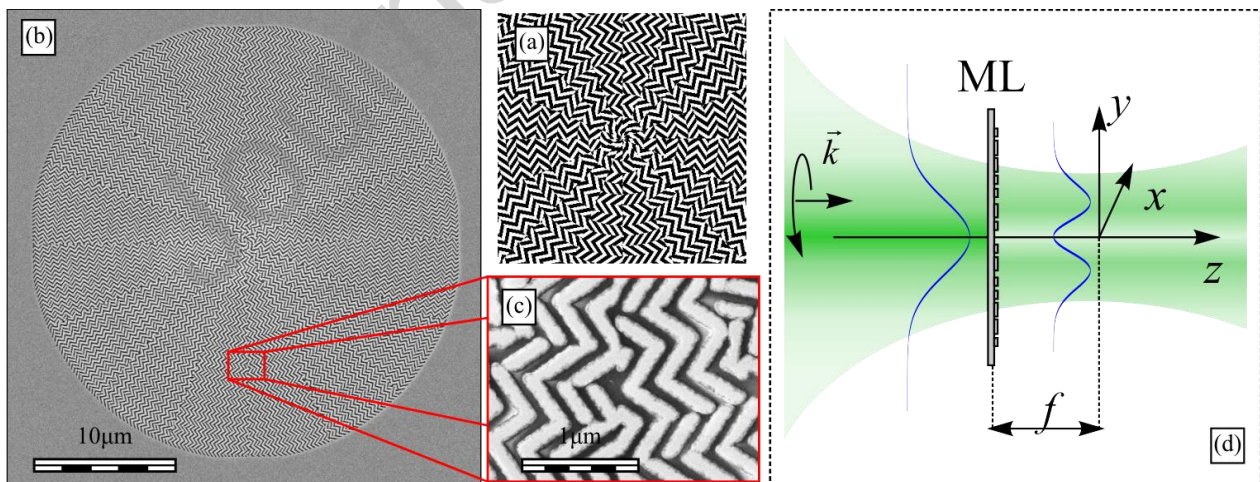


Fig. 1. (a) Template of the metalens under study, (b) SEM-image of the synthesized metalens and (c) a magnified fragment. (d) Schematic representation of a circularly polarized wave with wave-vector \vec{k} illuminating the metalens under analysis (ML) and near-focus ($f = \lambda$) Cartesian coordinates (x, y, z).

Figure 2 depicts the central fragment of an AFM-aided subwavelength microrelief pattern of the metalens in Fig. 1. The measurements have shown that an average height of the microrelief in an amorphous silicon film is 120 nm, with the maximum height gradient being 150 nm.

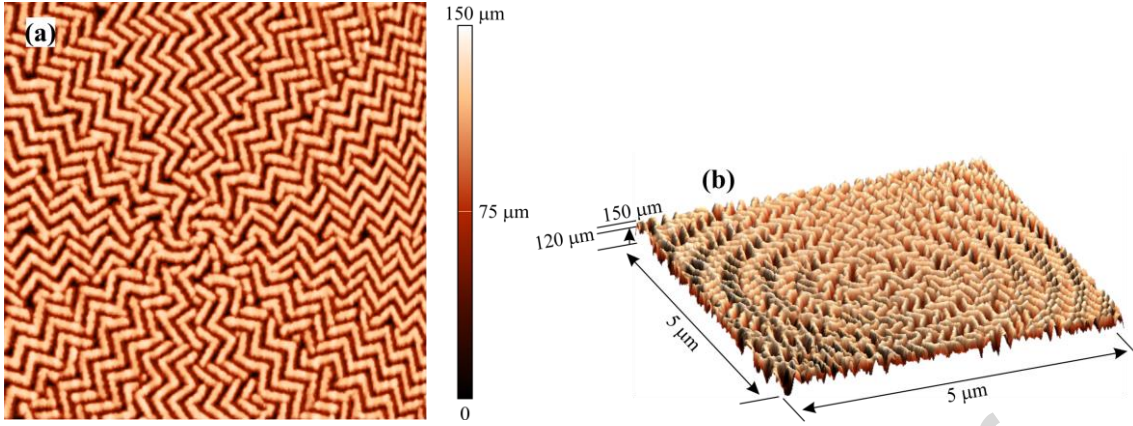


Fig. 2. (a) An AFM-aided pattern of the metalens central fragment (5x5 μm) and (b) its reconstructed 3D model.

4. FDTD-aided numerical simulation of the metalens

The FDTD-aided numerical simulation implemented using the FullWave software [42] has shown that the metalens generates a reverse energy flow when illuminated by light of an arbitrary polarization, be it linear, right- or left-handed circular polarization. The computations were conducted for a $\lambda/30$ mesh along all three axes, with the initial field containing 601x601 pixels for an 8x8- μm area. Figure 3 depicts the arguments (phases) of the transverse E-vector projections E_x and E_y (Figs. 3a and 3b) in the strong focus of the metalens in Fig. 1a illuminated by a Gaussian beam with the left-handed circular polarization. From Fig. 3a,b, the phase is seen to take a value of 4π as the polar angle makes a full circle around the central point. Hence, the optical vortex shaped has topological charge $m=2$. From Fig. 3a, b, the two projections of the electric field, E_x и E_y , are seen to have a phase shift of $\pi/2$. Hence, after passing through the metalens, the field acquires the right-handed circular polarization. Under illumination by the light with linear x -polarization, the metalens generates, in the focus, a linearly polarized field whose distribution is marked by arrows in Fig. 3c. From Fig. 3c, a 2nd-order cylindrical vector beam is seen to form at the output of the metalens of Fig. 1a, with the polarization vectors rotating about two points.

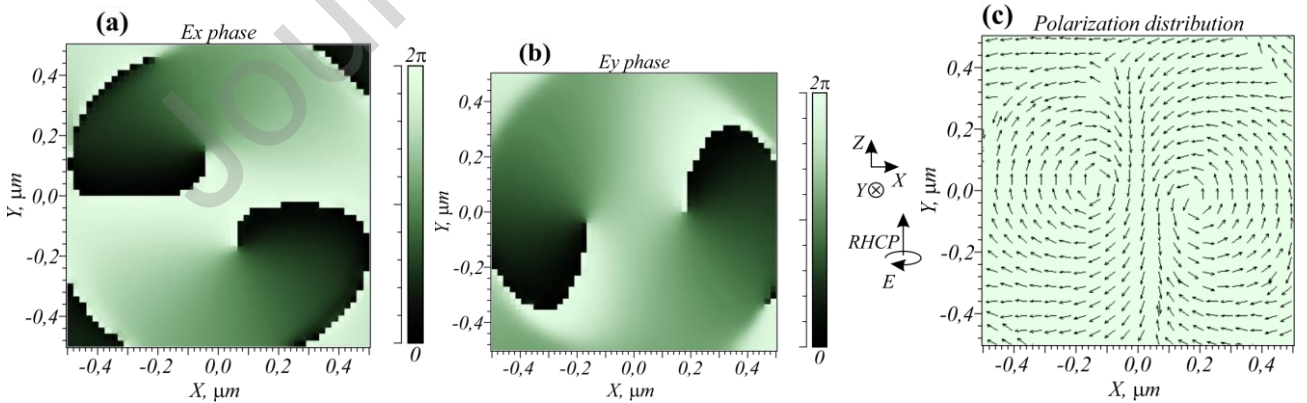


Fig. 3 FDTD-aided phase patterns of the transverse E-field components (a) E_x and (b) E_y in the focus of the metalens in Fig. 1a from an incident Gaussian beam with right-handed circular polarization. (c) Streamline map for linear polarization vectors in the metalens focus from an incident beam with linear horizontal x -polarization (E_x).

While directly measuring phase in the subwavelength focus would be challenging, it is possible to measure the focal intensity pattern. This fact has prompted us to obtain a numerically simulated intensity pattern near the metalens focus.

Figure 4 shows intensity patterns $I=I_x+I_y+I_z$ generated in the metalens focus located 400-nm away from its surface, the longitudinal component S_z of the Poynting vector $\mathbf{S}=\text{Re}[\mathbf{E}^* \times \mathbf{H}]$, and the transverse intensity component I_x+I_y . Below, the color bars on the right of Figs. 4-7 give relative units, with the intensity and the on-axis energy flow assumed to be unitary in all cases. Thus, the numbers in the color bars show the ratio of the energy and the energy flow to the incident ones. From Fig. 4(a-c), the intensity in the focus is seen to be annular-shaped for circular polarization or have two intensity peaks for linear polarization. The intensity in Fig. 4(g-i) is non-zero at the center, which is particularly clear when looking at the transverse component. From Fig. 4(d-f), it is seen that in all cases the maximum negative energy flow is at the center. Figure 4(g-i) provides better agreement with the experiment because the metallic pyramid probe of the scanning near-field optical microscope measures the near-focus transverse intensity of light [43], with the on-axis intensity at the center seen to be non-zero. Figure 5 depicts similar plots, including the total intensity, the transverse intensity, and the longitudinal projection of the Poynting vector along the propagation axis z when focusing right-handed circularly polarized incident light (thanks to symmetry, the distributions in the XZ and YZ planes are almost the same).

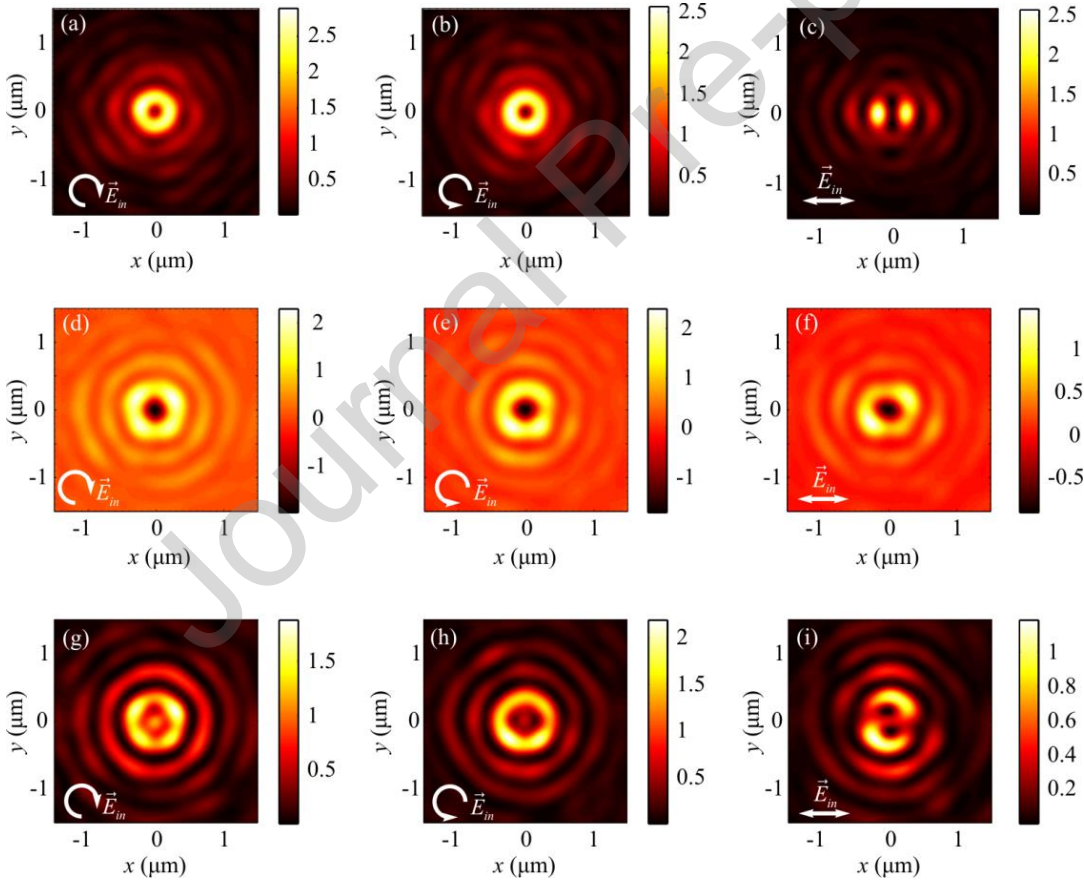


Fig. 4. Patterns of the intensity $I=I_x+I_y+I_z$ (a-c), the longitudinal component S_z of the Poynting vector (d-f), and the transverse intensity I_x+I_y (g-i) in the metalens focal plane (Fig. 1a) for the incident light with (a,d,g) right-handed circular, (b,e,h) left-handed circular, and (c,f,i) linear polarization.

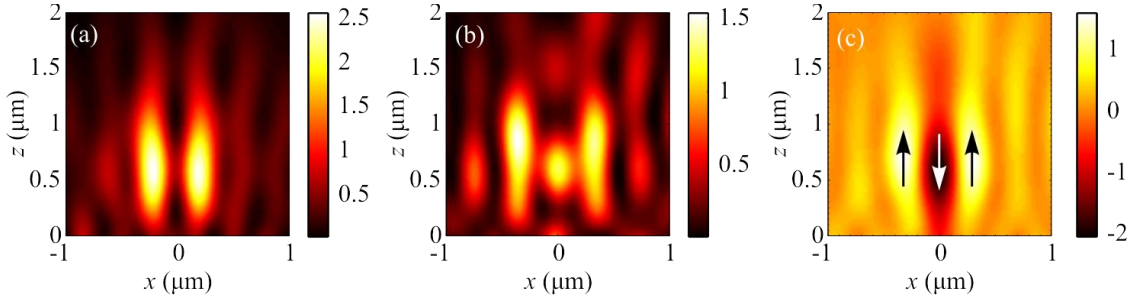


Fig. 5. Distribution of (a) the total intensity, (b) transverse intensity component, and (c) on-axis longitudinal component of the Poynting vector near the focus of the metalens (Fig. 1a) for the right-handed circularly polarized incident light.

From Fig. 5, the intensity pattern (Fig. 4a) and the longitudinal component of the Poynting vector in the transverse plane XY (Fig. 4c) are seen to always be doughnut-shaped. The total on-axis intensity (Fig. 4a) is characterized by alternating zero and non-zero values. The longitudinal on-axis component of the Poynting vector always takes negative values (Fig. 4c). Meanwhile the transverse intensity component (Fig. 4b) has a different intensity pattern in the transverse planes, being characterized by alternating bright intensity rings and peaks.

The negative on-axis energy flow occurs as the Poynting vector is composed of two vectors [44] – one being the canonical energy flow and the other – spin flow. Thus, the resulting energy flow (the on-axis component of the Poynting vector) in the focus in Fig. 5c is negative because the spin flow is negative and larger in magnitude than the always positive canonical component, which is proportional to the transverse intensity (Fig.5b).

Figure 6 depicts focal intensity patterns generated by linearly polarized light in the XZ and YZ planes. From Figs. 6(a) and Fig. 6(b), the intensity distribution is seen to be in the form of an asymmetric ring. Similar asymmetry, though less pronounced, is observed for the projection of the Poynting vector.

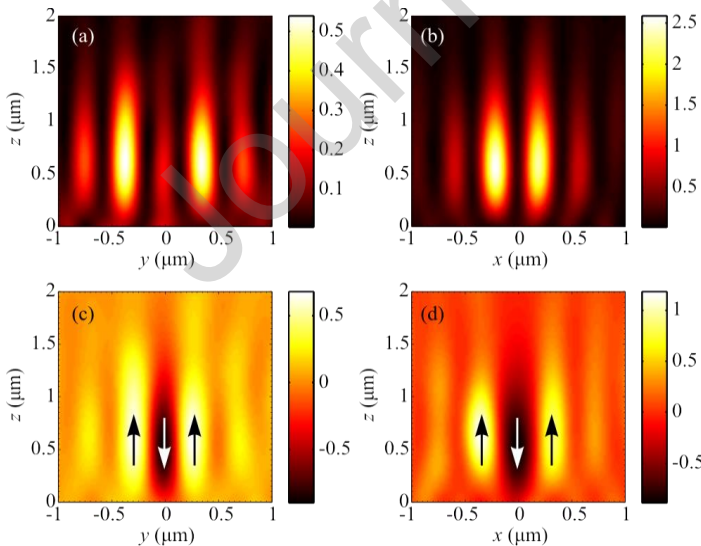


Fig. 6. On-axis intensity patterns from the metalens (Fig. 1a) in the planes (a) YZ and (b) XZ and the longitudinal projection of the Poynting vector in the planes (c) YZ and (d) XZ when focusing an incident wave linearly polarized along the X-axis.

5. Experiment

While being unable to directly measure the reverse energy flow, we are still able to demonstrate experimentally its presence in a certain region. In this work, aiming to detect a reverse energy flow near the optical metasurface, we utilized a hollow metal pyramid probe with a 100-nm nanohole in its tip. The probe was placed in the region where the reverse energy flow was expected, and scanning performed with a 35-nm step. We note that such a probe measures a transverse intensity and not an energy flow, being insensitive to the longitudinal intensity. Having found the transverse intensity to be non-zero, we concluded that the agreement between the calculated and probe-measured transverse intensity distributions serves to prove the presence of a reverse energy flow in the focus of the optical metalens. What is more important, the agreement between the calculated and experimentally measured intensity distributions was demonstrated for two types of beams – when focusing a circularly polarized second-order optical vortex and a non-vortex beam with second-order azimuthal polarization.

The metalens-aided focusing of laser light (Fig. 1b) was experimentally studied using a scanning near-field optical microscope (SNOM, Fig 7a).

In the experiment, a 80-mW laser beam of wavelength $\lambda = 633$ nm from a Cobolt 06 MLD laser was filtered using a 50-nm pinhole PH and a lens L_1 ($f_1 = 150$ mm), before passing through a linear polarization converter P_1 to obtain linearly polarized light. If a circularly polarized laser beam was to be obtained, a quarter-wavelength plate was placed behind the linear polarization converter. The beam was then focused onto a metalens using a lens L_2 ($f_2 = 10$ mm). The intensity distribution of light after passing through the metalens was measured with a cantilever C_1 (with a 100-nm nanohole, SNOM_C, NT-MDT). After passing through the cantilever, the light consecutively went through an objective lens O_1 (100X Mitutoyo Plan Apo Infinity Corrected Long WD Objective) and a spectrometer S_1 (Solar TII, Nanofinder 30) to filter out the irrelevant radiation, before being finally registered with a CCD camera (Andor, DV401-BV).

In the experiment, we demonstrated that when illuminated by the circularly polarized light, the metalens in Fig. 1b generated, at a distance of $0.4 - 0.5$ μm from the surface, a transverse annular intensity pattern of average diameter 800 nm (Fig. 7b). As the distance from the metalens increased to about $0.6 - 0.7$ μm , a local intensity peak of width $\text{FWHM}=0.6\lambda$ appeared at the center of the intensity pattern (Fig. 7c), before the pure-annular intensity pattern reappeared at a distance of $0.8 - 0.9$ μm . Such alternating patterns of intensity rings and peaks suggest that the SNOM-measured intensity distribution is in agreement with the numerically simulated transverse intensity distribution of Fig. 5b. For convenience, the SNOM-measured (Fig. 7b,d) and numerically simulated transverse intensity patterns (Fig. 7c,e) are juxtaposed.

From the comparison of Figs. 7b and 7c, the experimentally measured intensity ring is seen to be larger in diameter ($\text{FWHM}=0.81$ μm) than the numerically simulated one ($\text{FWHM}=0.66$ μm). This can be explained by the fact that the metalens used in the experiment had a larger diameter (30 μm) than that of the incident circularly polarized Gaussian beam.

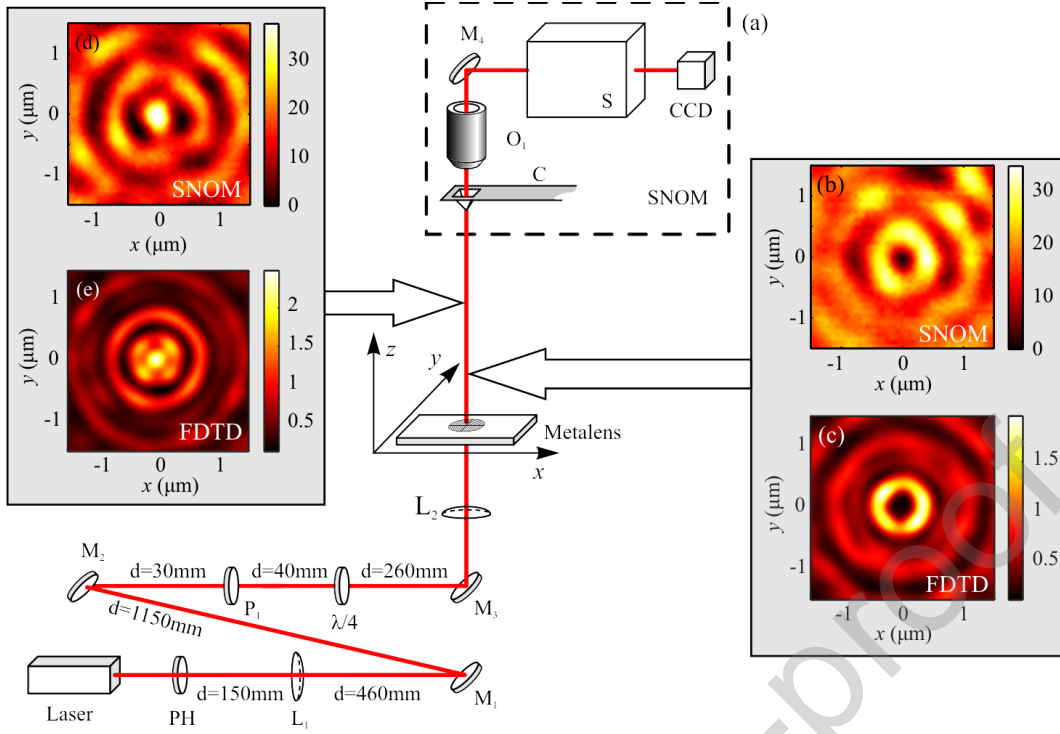


Fig. 7. Experimental setup. Laser – Cobolt 06 MLD ($\lambda = 633$ nm, 80 mW), P_1 – linear polarizer, L_1 , L_2 – lenses ($f_1 = 150$ mm and $f_2 = 10$ mm), PH– a pinhole (50 μm), M_1 , M_2 , M_3 , M_4 – mirrors, C– a cantilever (diameter 100 nm, SNOM_C, NT-MDT), O_1 – a 100 \times objective lens (100X Mitutoyo Plan Apo Infinity Corrected Long WD Objective), S – a spectrometer (Solar TII, Nanofinder 30), CCD – CCD camera (Andor, DV401-BV). (b,d) SNOM-measured and (c, e) numerically simulated distributions of the transverse intensity I_x+I_y from the metalens (Fig. 1) at a distance of (a,c) 0.4 μm (focus) and (b,d) 0.6 μm . The metalens was illuminated by a focused left-handed circularly polarized Gaussian beam.

A comparison of the experimental (Fig. 7b,d) and numerically simulated (Fig. 5c,e) intensity patterns in the metalens focus shows them to be in qualitative agreement. However, there are quantitative differences between them, which may be caused by A) metalens fabrication errors (Fig. 1b), B) failure to accurately generate the required diameter of the incident beam, C) failure to accurately measure the distance to the metalens surface (the error of about 100 nm), and D) intensity measurement error with a cantilever, which may introduce perturbations into the light field. However, the qualitative agreement between the experiment and simulation results in Fig. 7 indirectly proves that a reverse energy flow occurs near the metalens focus. We maintain that our experiment proves the existence of an on-axis reverse energy flow as the transverse intensity in the focus is non-zero. It has been theoretically shown [45] that when focusing a circularly/linearly polarized optical vortex with arbitrary integer topological charge m , the on-axis intensity has always been zero, except for when $m=2$. Thus, upon creating an optical vortex, a non-zero on-axis transverse intensity in the focus has been an indicator of a reverse on-axis energy flow. It is not possible to directly measure the reverse flow in the focus of the metalens using a SNOM probe because the SNOM probe measures the transverse intensity rather than measuring the energy flow [43]. The conclusion that it is the transverse intensity I_x+I_y in the focus that the metallic SNOM probe predominantly measures can be drawn from the Bethe-Bouwkamp theory [46]. The theory states that when illuminating a metallic screen with a nanohole of diameter a much smaller than the incident wavelength λ , a light wave with the electric vector \mathbf{E} induces an electric dipole \mathbf{P} and magnetic dipole \mathbf{M} within the nanohole:

$$\mathbf{P} = -\frac{4}{3}\epsilon_0 a^3 (\mathbf{E}\mathbf{n}_z)\mathbf{n}_z, \quad \mathbf{M} = -\frac{8}{3}a^3 [\mathbf{n}_z \times [\mathbf{E} \times \mathbf{n}_z]] \quad (11)$$

where \mathbf{n}_z is a unit vector perpendicular to the nanohole which is parallel to the optical axis z and ε_0 is the vacuum permittivity. From (11), the electric dipole \mathbf{P} is seen to be contributed to by the longitudinal E-field component E_z , irradiating in the transverse direction and not to be detected by the photoreceiver located on the z -axis. On the contrary, the magnetic dipole \mathbf{M} is contributed to only by the transverse E-field components (E_x, E_y), irradiating along the optical axis z . Hence, we infer that the photodetector signal is proportional to the radiation of the magnetic dipole \mathbf{M} , which is proportional to the transverse field intensity: I_x+I_y .

Meanwhile the direct measurement of the reverse energy flow in the focus of a microlens with NA=0.95 has been reported [30].

Below, we discuss focusing a linearly polarized laser beam. The SNOM-measured intensity distribution in the focus ($0.4 \mu\text{m}$ behind the metalens) is depicted in Fig. 6a.

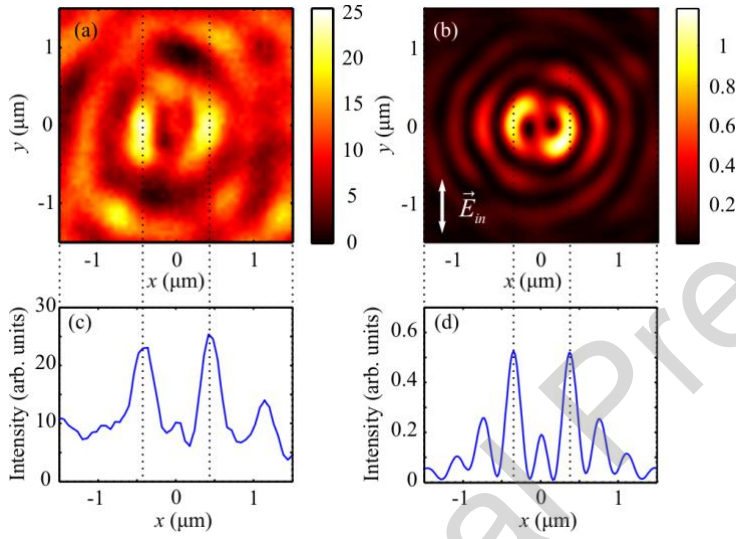


Fig.8. Transverse intensity patterns in the focus of the metalens in Fig. 1 at a distance of $0.4 \mu\text{m}$ from its surface: (a) SNOM-measured and (b) numerically simulated. The metalens was illuminated with a Gaussian beam linearly polarized along the X axis. Transverse intensity profile in the metalens focus obtained along the Y-axis by (c) SNOM measurements (Fig. 8a) and (d) numerical simulation (Fig. 8b).

From Fig. 6, the intensity pattern is seen to have two peaks located $0.87 \mu\text{m}$ apart (Fig. 6a), with a non-zero intensity found at the center. For a more detailed comparison, Fig. 6cd depicts Y-axis profiles of the transverse intensity distribution $0.4 \mu\text{m}$ behind the metalens of Fig. 1(a), which were measured with a SNOM (Fig. 6a) and (b) numerically simulated (Fig. 6b). A comparison of the experimental and numerically simulated results in Fig. 6 shows them to be in qualitative agreement. A difference between the numerically simulated and experimentally measured results is due to SNOM-probe introduced perturbations of the light field. However, the qualitative agreement between the intensity patterns obtained in the experiment and via the FDTD-aided numerical simulation indirectly proves that when illuminated by the linearly polarized light, the metalens of Fig. 1 produces an on-axis near-focus reverse energy flow.

Conclusion

A high-NA metalens synthesized in a thin-film amorphous silicon and intended to generate a reverse energy flow in the strong focus of laser light has been experimentally characterized. Such a metalens has been synthesized and characterized for the first time. Its unique feature is that when illuminated by an arbitrary beam with homogeneous (linear, right- or left-handed circular) polarization, the metalens generates an on-axis near-focus reverse energy flow. The $30\text{-}\mu\text{m}$ metalens combined a spiral Fresnel

zone plate, whose focal length was equal to the incident wavelength of 633 nm (400 nm, in the experiment), and a 16-sectored polarization converter composed of spatially varying binary subwavelength diffraction gratings of period 220 nm, synthesized in a thin-film amorphous silicon. The 16-sectored polarization converter has been shown to convert a linearly polarized incident laser beam into a cylindrical second-order vector beam, also converting a right(left)-handed circularly polarized incident beam into a right(left)-handed circularly polarized optical vortex with topological charge $m = -2$ ($m = 2$). The metalens proposed here has similar parameters to a metalens from Ref. [39], but ours is the shortest focus length metalens, demonstrated to date.

The near-surface intensity distributions were measured using a SNOM with a hollow metallic pyramid-shaped probe with a 100-nm pinhole in its vertex. The metalens has been experimentally shown to generate a doughnut intensity profile in the strong focus if illuminated by a circularly polarized light, generating two intensity peaks if illuminated by the linearly polarized light. The intensity patterns obtained in the experiment and via the FDTD-aided numerical simulation are in qualitative agreement. Based on this agreement, we may infer that the metalens under study operates in the intended way, generating a near-focus reverse energy flow for both circularly and linearly polarized incident light.

Acknowledgments

The work was partly funded by the Russian Federation Ministry of Science and Higher Education within a government project of the FSRC “Crystallography and Photonics” of the RAS, the Russian Science Foundation under grant 18-19-00595 (experiment), the Russian Foundation for Basic Research under grant # 18-29-20003 (numerical simulation), EU H2020 Marie Skłodowska-Curie TERRIFIC grant agreement no. 749143, and the European Union's Horizon 2020 Research and Innovation programme via ASCENT Access Network, grant agreement no. 654384 (metalens fabrication) and Science Foundation Ireland under Grant SFI12/RC/2276_P2.

References

1. A. Arbabi, Y. Horie, A. J. Ball, M. Bagheri, and A. Faraon, "Subwavelength-thick lenses with high numerical apertures and large efficiency based on high-contrast transmitarrays," *Nat. Commun.* **6**, 7069 (2015).
2. A. Arbabi, Y. Horie, M. Bagheri, and A. Faraon, "Dielectric metasurfaces for complete control of phase and polarization with subwavelength spatial resolution and high transmission," *Nat. Nanotechnol.* **10**, 937–943 (2015).
3. F. Aieta, P. Genevet, M. A. Kats, N. Yu, R. Blanchard, Z. Gaburro, and F. Capasso, "Aberration-Free Ultrathin Flat Lenses and Axicons at Telecom Wavelengths Based on Plasmonic Metasurfaces," *Nano Lett.* **12**, 4932–4936 (2012).
4. X. Ni, S. Ishii, A. V. Kildishev, and V. M. Shalaev, "Ultra-thin, planar, Babinet-inverted plasmonic metalenses," *Light Sci. Appl.* **2**, e72 (2013).
5. P. R. West, J. L. Stewart, A. V. Kildishev, V. M. Shalaev, V. V. Shkunov, F. Strohkendl, Y. A. Zakharenkov, R. K. Dodds, and R. Byren, "All-dielectric subwavelength metasurface focusing lens," *Opt. Express* **22**, 26212–26221 (2014).
6. D. Lin, P. Fan, E. Hasman, and M. L. Brongersma, "Dielectric gradient metasurface optical elements," *Science* **345**, 298–302 (2014).
7. Q. Fan, M. Liu, C. Yang, L. Yu, F. Yan, and T. Xu, "A high numerical aperture, polarization-insensitive metalens for long-wavelength infrared imaging," *Appl. Phys. Lett.* **113**, 201104 (2018).
8. I. Tanriover and H. V. Demir, "Broad-band polarization-insensitive all-dielectric metalens enabled by intentional off-resonance waveguiding at mid-wave infrared," *Appl. Phys. Lett.* **114**, 043105 (2019).
9. L. Lan, W. Jiang, and Y. Ma, "Three dimensional subwavelength focus by a near-field plate lens," *Appl. Phys. Lett.* **102**, 231119 (2013).

10. S. S. Stafeev, V. V. Kotlyar, A. G. Nalimov, M. V. Kotlyar, and L. O'Faolain, "Subwavelength gratings for polarization conversion and focusing of laser light," *Photonics Nanostructures - Fundam. Appl.* **27**, 32–41 (2017).
11. V. Kotlyar, S. S. Stafeev, A. G. Nalimov, and L. O'Faolain, "Subwavelength grating-based spiral metalens for tight focusing of laser light," *Appl. Phys. Lett.* **114**, 141107 (2019).
12. Y. Yu, H. Huang, M. Zhou, and Q. Zhan, "Engineering of multi-segmented light tunnel and flattop focus with designed axial lengths and gaps," *Opt. Commun.* **407**, 398–401 (2018).
13. C. Zheng, S. Su, H. Zang, Z. Ji, Y. Tian, S. Chen, K. Mu, L. Wei, Q. Fan, C. Wang, X. Zhu, C. Xie, L. Cao, and E. Liang, "Characterization of the focusing performance of axial line-focused spiral zone plates," *Appl. Opt.* **57**, 3802–3807 (2018).
14. J. Lin, R. Chen, P. Jin, M. Cada, and Y. Ma, "Generation of longitudinally polarized optical chain by 4π focusing system," *Opt. Commun.* **340**, 69–73 (2015).
15. Y. Yu and Q. Zhan, "Generation of uniform three-dimensional optical chain with controllable characteristics," *J. Opt.* **17**, 105606 (2015).
16. X. Wang, B. Zhu, Y. Dong, S. Wang, Z. Zhu, F. Bo, and X. Li, "Generation of equilateral-polygon-like flat-top focus by tightly focusing radially polarized beams superposed with off-axis vortex arrays," *Opt. Express* **25**, 26844 (2017).
17. H. Chen, S. Tripathi, and K. C. Toussaint, "Demonstration of flat-top focusing under radial polarization illumination," *Opt. Lett.* **39**, 834 (2014).
18. V. V. Kotlyar, S. S. Stafeev, and A. A. Kovalev, "Reverse and toroidal flux of light fields with both phase and polarization higher-order singularities in the sharp focus area," *Opt. Express* **27**, 16689–16702 (2019).
19. V. V. Kotlyar, A. A. Kovalev, and A. G. Nalimov, "Energy density and energy flux in the focus of an optical vortex: reverse flux of light energy," *Opt. Lett.* **43**, 2921–2924 (2018).
20. S. S. Stafeev, V. V. Kotlyar, A. G. Nalimov, and E. S. Kozlova, "The Non-Vortex Inverse Propagation of Energy in a Tightly Focused High-Order Cylindrical Vector Beam," *IEEE Photonics J.* **11**, 4500810 (2019).
21. H. Lv, X. Lu, Y. Han, Z. Mou, S. Tang "Multi-focal metalens with a controllable intensity ration," *Opt. Lett.* **44**, 2518-2521 (2019).
22. W.T. Chen, A.Y. Zhu, J. Sisler, Z. Bharwani, F.A. Capasso "A broadband achromatic polarization-intensitive metalens consisting of anisotropic nanostructures," *Nat. Commun.* **10**, 1-7 (2019).
23. R. Lin, X. Li "Multifocal metalens based on multilayer Pancharatnam-Berry phase elements architecture," *Opt. Lett.* **44**, 2819-2822 (2019).
24. S. Tian, H. Guo, J. Hu, S. Zhuang "Dielectric longitudinal bifocal metalens with adjustable intensity and high focusing efficiency," *Opt. Express* **27**, 680-688 (2019).
25. B. Huang, W. Bai, H. Jia, J. Han, P. Guo, J. Wu, J. Yang "Multifocal co-plane metalens based on computer-generated holography for multiple visible wavelengths," *Results in Phys.* **17**, 103085 (2020).
26. H. Chung, D. Kim, A. Sawant, I. Lee, E. Choi, J. Lee "Generation of E-band metasurface-based vortex beam with reduced divergence angle," *Sci Rep.* **10**, 8289 (2020).
27. J. Engelberg, U. Levy "The advantages of metalenses over diffractive lenses," *Nat. Commun.* **11**, 1991 (2020).
28. V. V. Kotlyar, A. G. Nalimov, S. S. Stafeev, and L. O'Faolain, "Single metalens for generating polarization and phase singularities leading to a reverse flow of energy," *J. Opt.* **21**, 055004 (2019).
29. S. Slussarenko, A. Muravski, T. Du, V. Chigrinov, L. Marrucci, E. Santamato "Tunable liquid crystal q-plates with arbitrary topological charge," *Opt. Express* **19**, 4085-4090 (2011).
30. V. V. Kotlyar, S. S. Stafeev, A. G. Nalimov, A. A. Kovalev, and A. P. Porfirev, "Mechanism of formation of an inverse energy flow in a sharp focus," *Phys. Rev. A* **101**, 033811 (2020).
31. Richards, E. Wolf "Electromagnetic diffraction in optical systems. II. Structure of the image field in an aplanatic system". *Proc. R. Soc. London Ser. A* **253**, 358–379 (1959).

32. M. Khorasaninejad, W. T. Chen, R. C. Devlin, J. Oh, A. Y. Zhu, and F. Capasso, "Metalenses at visible wavelengths: Diffraction-limited focusing and subwavelength resolution imaging," *Science* **352**, 1190–1194 (2016).
33. M. Khorasaninejad, A. Y. Zhu, C. Roques-Carmes, W. T. Chen, J. Oh, I. Mishra, R. C. Devlin, and F. Capasso, "Polarization-Insensitive Metalenses at Visible Wavelengths," *Nano Lett.* **16**, 7229–7234 (2016).
34. W. T. Chen, A. Y. Zhu, V. Sanjeev, M. Khorasaninejad, Z. Shi, E. Lee, and F. Capasso, "A broadband achromatic metalens for focusing and imaging in the visible," *Nat. Nanotechnol.* **13**, 220–226 (2018).
35. A. Zhan, S. Colburn, R. Trivedi, T. K. Fryett, C. M. Dodson, and A. Majumdar, "Low-Contrast Dielectric Metasurface Optics," *ACS Photonics* **3**, 209–214 (2016).
36. B. H. Chen, P. C. Wu, V.-C. Su, Y.-C. Lai, C. H. Chu, I. C. Lee, J.-W. Chen, Y. H. Chen, Y.-C. Lan, C.-H. Kuan, and D. P. Tsai, "GaN Metalens for Pixel-Level Full-Color Routing at Visible Light," *Nano Lett.* **17**, 6345–6352 (2017).
37. S. Wang, P. C. Wu, V. C. Su, Y. C. Lai, M. K. Chen, H. Y. Kuo, B. H. Chen, Y. H. Chen, T. T. Huang, J. H. Wang, R. M. Lin, C. H. Kuan, T. Li, Z. Wang, S. Zhu, and D. P. Tsai, "A broadband achromatic metalens in the visible," *Nat. Nanotechnol.* **13**, 227–232 (2018).
38. J. Xu, M. Cua, E.H. Zhou, Y. Hori, A. Faraon, C. Yang "Wide-angular-range and high-resolution beam steering by a metasurface-coupled phase array," *Opt. Lett.* **43**, 5255–5258 (2018).
39. R. Paniagua-Domínguez, Y. F. Yu, E. Khaidarov, S. Choi, V. Leong, R.M. Bakker, X. Liang, Y.H. Fu, V. Valuckas, L.A. Krivitsky, A. I. Kuznetsov "Metalens with a near-unity numerical aperture," *Nano Lett.* **18**, 2124–2132 (2018).
40. Z. Zhou, J. Li, R. Su, B. Yao, H. Fang, K. Li, L. Zhou, J. Liu, D. Stellinga, C. P. Reardon, T. F. Krauss, and X. Wang, "Efficient Silicon Metasurfaces for Visible Light," *ACS Photonics* **4**, 544–551 (2017).
41. H. Li, B. Fang, C. Chen, S. Zhu, T. Li "Cavity-enhanced metallic metalens with improved efficiency," *Sci Rep.* **10**, 417 (2020).
42. www.synopsys.com/photonic-solutions/rsoft-photonic-device-tools/passive-device-fullwave.html
43. V. V. Kotlyar, S. S. Stafeev, Y. Liu, L. O'Faolain, and A. A. Kovalev, "Analysis of the shape of a subwavelength focal spot for the linearly polarized light," *Appl. Opt.* **52**, 330–339 (2013).
44. M.V. Berry "Optical currents," *J. Opt. A: Pure Appl. Opt.* **11**, 094001 (2009).
45. V.V. Kotlyar, A.G. Nalimov, S.S. Stafeev «Exploiting the circular polarization of light to obtain a spiral energy flow at the subwavelength focus, " *J. Opt. Soc. Am. B.* **36**, 2850–2855 (2019)
46. J.H. Wu "Modeling of near-field optical diffraction from a subwavelength aperture in the conducting film," *Opt. Lett.* **36**, 3440–3442 (2011).

Highlights

- We fabricate a spiral metalens that is composed of 16-sectored subwavelength binary gratings.
- Near-focus intensity distributions was measured by a scanning near-field optical microscope.
- The near-focus reverse energy flow is experimentally confirmed to occur.

Declaration of interests

The authors declare that they have no known competing financial interests or personal relationships that could have appeared to influence the work reported in this paper.

The authors declare the following financial interests/personal relationships which may be considered as potential competing interests:

Journal Pre-proof